Improved Confinement with Reversed Magnetic Shear in TFTR

F. M. Levinton,[1] M. C. Zarnstorff,[2] S. H. Batha,[1] M. Bell,[2] R. E. Bell,[2] R. V. Budny,[2] C. Bush,[3] Z. Chang,[2] E. Fredrickson,[2] A. Janos,[2] J. Manickam,[2] A. Ramsey,[2] S. A. Sabbagh,[4] G. L. Schmidt,[2] E. J. Synakowski,[2] and G. Taylor[2]

[1]*Fusion Physics and Technology, Torrance, California 90503*

[2]*Princeton Plasma Physics Laboratory, Princeton, New Jersey 08543*

[3]*Oak Ridge National Laboratory, Oak Ridge, Tennessee 37831*

[4]*Columbia University, New York, New York 10027*

(Received 23 May 1995)

A new tokamak confinement regime has been observed on the Tokamak Fusion Test Reactor (TFTR) where particle and ion thermal diffusivities drop precipitously by a factor of ~40 to the neoclassical level for the particles and to much less than the neoclassical value for the ions in the region with reversed shear. This enhanced reversed shear confinement mode allows the central electron density to rise from 0.45×10^{20} m^{-3} to $\sim 1.2 \times 10^{20}$ m^{-3} with $T_i \sim 24$ keV and $T_e \sim 8$ keV. This regime holds promise for significantly improved tokamak performance.

PACS numbers: 52.55.Fa, 52.30.Bt

The economic attractiveness of the tokamak as a candidate for a fusion reactor depends on the development of a magnetic configuration that has good confinement, stability, and low recirculating power for a steady state current drive. This requires a high fraction of self-sustaining bootstrap current that is well aligned with an optimized current density profile for confinement and stability. Recent studies [1,2] of the optimization of the current density profile suggest that reversed magnetic shear (i.e., a hollow current density profile) is desirable for confinement, stability, and bootstrap alignment. Shear is defined as $s \equiv (2V/q)(dq/d\psi)(d\psi/dV) \approx (r/q)(dq/dr)$, where ψ is the enclosed poloidal flux, V is the enclosed volume, q is the safety factor, and r is the minor radius. Reversed shear, $s < 0$, is thought to be important because it can stabilize some classes of microinstabilities such as trapped electron modes [3,4], a candidate to explain the observed anomalous electron transport in tokamaks. Reversed magnetic shear can stabilize some magnetohydrodynamic (MHD) instabilities such as ballooning modes [5] and resistive tearing modes and is also considered important for the stellarator magnetic configuration [6]. If improved core confinement can be attained, the high pressure gradient would generate a strong off-axis bootstrap current and sustain the hollow current density profile. This scenario may lead to an attractive concept for a steady state tokamak reactor [7]. Most tokamaks operate with inductive current drive, which normally produces a peaked current density profile at the magnetic axis due to the strong dependence of the plasma conductivity on the electron temperature. Only by noninductive current drive or transient techniques can a hollow current density profile be generated. This has been done in several experiments reporting improved confinement [8–12] and stability [13–15]. In addition, several other experiments have reported that stabilization of MHD modes in the high β_p regime [16–19] and β self-stabilization [20] can improve performance.

Recent experiments on the Tokamak Fusion Test Reactor (TFTR) [21] have demonstrated a reversed shear configuration with greatly improved particle and ion thermal transport in the reversed shear region that is more than an order of magnitude lower than reported in previous experiments, including reversed shear experiments. This regime of operation holds promise for significantly improving the tokamak reactor concept and can lead to a dramatic increase in the performance of present tokamaks. The $q(R, t)$ profile is obtained from the motional Stark effect (MSE) polarimeter [22,23] measurement of the local magnetic field pitch, in contrast to the indirect methods used in many previous experiments. The diagnostic provides good temporal and spatial resolution and shows the correlation of the magnetic shear with changes in transport and stability.

In the plasmas discussed here, reversed shear is created during the plasma startup phase. A deuterium plasma is ramped up in current at a ramp rate of 1.8 MA/s to about 1.0 MA. The rate of rise of the plasma current is then reduced to 0.4 MA/s until the final plasma current of $I_p = 1.6$ MA is reached, as shown in Fig. 1. The major radius is 2.60 m, the minor radius is 0.94 m, and the toroidal field is 4.6 T with an edge safety factor of ~6.2. Since the current diffusion time is much longer than the rise time of the plasma current, a hollow current density profile is formed. To further retard the current penetration to the plasma center, neutral beam injection (NBI) begins with a low power (5–7.5 MW) phase at ~0.6 s, heating the electrons from ~2 to ~5 keV and thereby increasing the current diffusion time to ~10 s. Neutral beam injection, cotangential to the plasma current, is also used in the early low power phase to drive a significant fraction of the plasma current. The high power heating phase then follows, as shown in Fig. 1, with up to 25 MW of NBI. Typical q profiles, prior to and during the high power phase are shown in Fig. 2. The profiles

0031-9007/95/75(24)/4417(4)$06.00

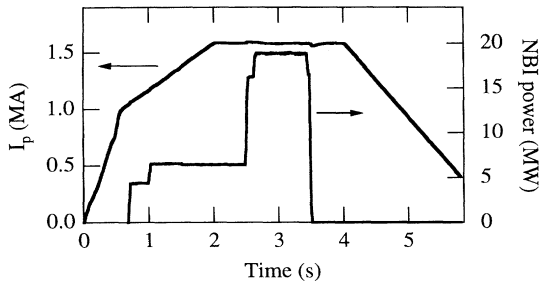

FIG. 1. The plasma current and neutral beam power evolution for a reversed shear startup.

have been reconstructed with the VMEC free-boundary equilibrium code [24] from the MSE data, kinetic pressure data, calculated fast ion pressure from the TRANSP code [25], and external magnetics data. The uncertainties in $q(R)$ are 10% or less across the profile [26]. The q profile has $q(0) \geq 4$–5, $q_{\min} \sim 3$, and $r_{\min}/a \sim 0.4$–0.5 at $t = 2.0$ s, the start of the I_p flattop, where $r_{\min}$ is the radius of $q_{\min}$. The quantities $q(0)$, $q_{\min}$, and $r_{\min}$ slowly decrease on a time scale of several seconds and reach $q(0) \sim 3$–4, $q_{\min} \sim 2$, and $r_{\min}/a \sim 0.3$ after 3 s of beam heating, consistent with the neoclassical current diffusion rate and the calculated driven currents. Initial reversed shear experiments in TFTR [7] were generated by a second current ramp-up after a 1.0 MA plasma was established. Those plasmas showed an improvement in transport similar to the plasmas discussed here.

Below NBI powers of 18 MW the plasmas formed in the reversed shear configuration phase appear to be similar to supershots [27], with a central ion temperature of ~24 keV, electron temperature of ~6–8 keV, and a central electron density of $\sim 4 \times 10^{19}$ m^{-3}. However, above an empirical threshold in neutral beam power, in the range of ~18–25 MW, the particle and thermal transport dramatically improve in the plasma core where the shear is reversed. The central electron density increases from $\sim 4 \times 10^{19}$ m^{-3} to $\sim 1.2 \times 10^{20}$ m^{-3} in ~0.3 s, as measured by a 10-channel interferometer array and shown in Fig. 3(a). The uncertainty of the central density is ~20%,

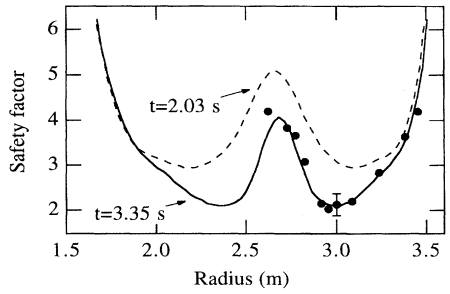

FIG. 2. The q profiles at the beginning of the current flattop at $t = 2$ s (dashed line), and near the end of the heating phase at $t = 3.35$ s (solid line).

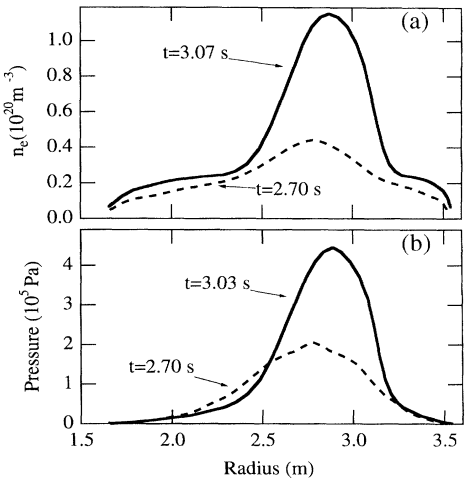

FIG. 3. The (a) density and (b) pressure profile before the transition to the ERS mode (dashed line) and at the time of peak density and pressure (solid line).

due to the large density gradient and lack of an interferometer chord at that location. The uncertainty is substantially smaller [28] for radii beyond the interferometer chord nearest the magnetic axis, which is located at $R = 2.99$ m or $r/a \sim 0.13$ at $t = 3.07$ s. The density profile outside the reversed shear region changes little, resulting in a peaked density profile. The transition to the highly peaked enhanced reversed shear (ERS) mode occurs abruptly during the discharge, within 0.2–0.9 s after the start of the high power heating phase. Shown in Fig. 4(a) is the evolution of the central density, with a transition into the ERS mode at $t = 2.715$ s. Also shown

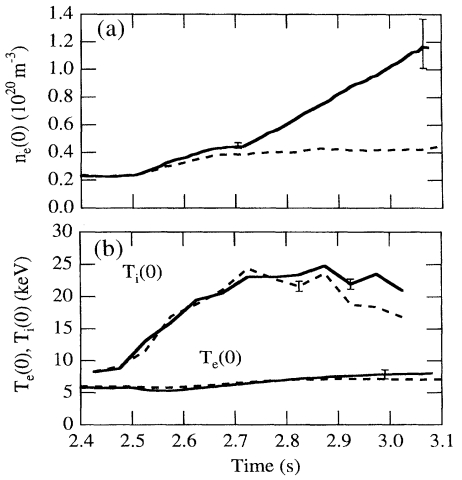

FIG. 4. The evolution of the electron density (a) and temperatures (b) at the magnetic axis for a discharge that makes a transition into the ERS mode at 2.715 s (solid line) and a similar reversed shear discharge at lower NBI power that does not (dashed line).

in Fig. 4(a) is a discharge without an ERS-mode transition, with an identical low power heating phase and similar reversed shear q profile, but lower NBI power in the high power heating phase. The high power heating phase starts at 2.5 s, with the neutral beam power increasing from 7 to 19 MW in the discharge that does not exhibit a transition into the ERS mode and to 25 MW in the discharge that does have a transition. In both cases the NBI is near balanced with a measured plasma rotation that is small. After the transition into the ERS mode, the electron temperature increases ~25% within the core region only, with little change outside, whereas the ion temperature profile is broadened. The central ion and electron temperature evolution is shown in Fig. 4(b). The resulting pressure profile, including the calculated fast ion contribution, shown in Fig. 3(b), is very peaked with a peaking factor, $F_p = p(0)/\langle p \rangle = 8.0$, where $p(0)$ is the pressure at the magnetic axis and $\langle p \rangle$ is the volume-averaged pressure. This is larger than the typical peaking factors for supershots of ~5 and for L-mode discharges of ~3.3. Because of the large measured pressure gradient, the calculated bootstrap current reaches ~75% of the total current. During the high power heating phase, the MSE measurements are obscured by spectral overlap from the different beams precluding a direct $q(R,t)$ measurement during this period. Just before the high power heating phase the measured q profiles are similar to those shown in Fig. 2, and the predicted poloidal field diffusion indicates that the q-profile evolution during the high power phase is similar to measured q profiles at lower NBI power. Once the plasma has transitioned into the ERS mode, it remains in this low transport regime, with the core plasma pressure rising linearly in time until either an MHD limit is reached, resulting in a disruption, or the neutral beam power is turned off or significantly reduced. In the latter case, after the neutral beam power has been turned off or reduced to ~5 MW the plasma remains in an ERS mode for ~0.2 s. During this time the ion temperature and stored energy drop appreciably before the plasma transitions out of the ERS mode.

A time-dependent transport analysis was performed using the TRANSP code. After the transition into the ERS mode the particle and ion thermal diffusivity drop precipitously throughout the region of reversed shear, which extends out to $r/a \sim 0.35$. The improved confinement extends beyond the reversed shear radius, into the region of reduced shear as well. The inferred particle diffusivity, D_e, assuming no pinch terms, drops by a factor of ~40 in the reversed shear region to roughly the neoclassical level or perhaps lower, as shown in Fig. 5(a). The ion thermal diffusivity, χ_i, analyzed assuming classical electron-ion energy exchange and no pinch term, also drops substantially to a level that is much less than the estimated neoclassical value, χ_i^{nc}, which is widely believed to be the irreducible minimum transport possible. Profiles of the inferred ion thermal diffusivity, before and after a transition into the ERS mode compared to estimated neoclassical ion thermal diffusivity, are shown in Fig. 5(b). The electron thermal diffusivity also drops by a factor of 2, but not in all discharges. In the particle and energy balance analysis it is found that the time rate of change of density and energy density are considerably larger than the radial losses. The sytematic and statistical uncertainties of the transport coefficients have been estimated. Their statistical variation over a period of 200 ms is used to determine the statistical standard deviation of the transport coefficients, which are computed every 10 ms. The systematic uncertainty is determined by calculating the uncertainty of each term in the transport equations from the propagation of the systematic uncertainties in the input power and kinetic profile data. The uncertainties shown in Fig. 5 reflect the combined statistical and systematic uncertainties. For example, the dominant radial loss term in the ion power balance is the electron-ion energy exchange, which is about 2 MW at $r/a = 0.2$ and has an uncertainty of ~5%.

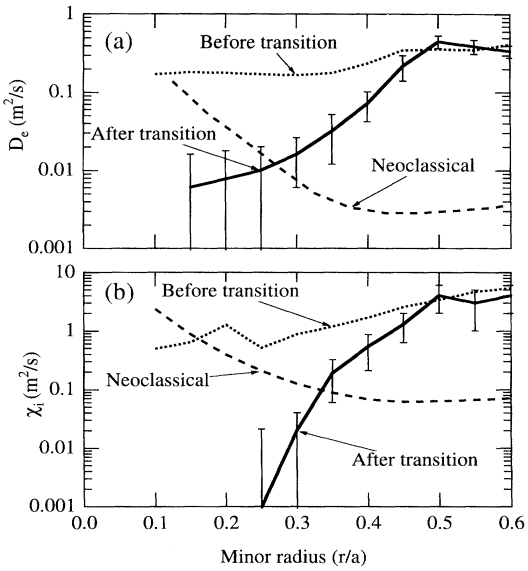

FIG. 5. The electron particle (a) and ion thermal (b) diffusivity profile before a transition (dotted line), at 2.6 s. The estimated neoclassical particle (a) and ion thermal (b) diffusivity (dashed line) and the particle (a) and ion thermal (b) diffusivity after a transition (solid line) are shown at 3.0 s. The region of reversed shear extends to $r/a \sim 0.35$.

The ion thermal diffusivity being less than that predicted by conventional neoclassical theory and the particle diffusivity being comparable to neoclassical is quite astounding. One possible rationalization of the observed subneoclassical ion thermal diffusivity is that the measured ion pressure gradient scale length is comparable to the ion thermal banana width, violating the assumptions of standard neoclassical theory. Other potential explanations include the existence of a large thermal pinch or an anomalous ion-electron thermal equilibration. Other enhanced perfor-

mance regimes [10,12,15,29], including other reversed shear experiments, have a particle and ion thermal diffusivity that are comparable to values present in the TFTR supershot phase *prior* to the transition to the ERS mode. After the transition to the ERS mode, both D_e and χ_i are reduced by a factor of 10–100 relative to the published values for these other regimes.

The reversed shear plasmas are observed to be free of any coherent, low-n or high-n MHD activity throughout the region of reversed shear. This includes the discharges with very peaked pressure profiles and large pressure gradients, $p' = dp/d\psi$, which are often the driving mechanism for MHD instabilities. The pressure gradient in the ERS mode is larger by a factor of 3–5 than in typical TFTR supershots. Supershots often have low-n MHD modes in the plasma core, identified as neoclassical tearing modes [30], which theoretically may be stabilized by reversed shear. The improved confinement in the reversed shear region is also consistent with recent theoretical predictions for the suppression of persistent microinstabilities driven by trapped particle dynamics and ion temperature gradient effects [1]. Outside the region of reversed shear, MHD modes are sometimes present and are currently limiting the stability and performance of the ERS mode to values of $\beta_N^* = 3.5$, where $\beta^* \equiv 2\mu_0\langle p^2\rangle^{1/2}/B_T^2$ and $\beta_N^* = \beta^* a B_T/I_p(MA)$, with B_T the vacuum toroidal field, in Tesla. The discharges with high performance develop an $n = 1$ internal mode and possibly a ballooning mode just outside the $q_{\min}$ radius before terminating in a disruption. Numerical calculations of the MHD stability predict an $n = 1$ infernal mode, consistent with the experimental observations. According to ideal MHD theory, the β_N^* limit is sensitive to the value of $q_{\min}$, $r_{\min}$, $q(0)$, and the total plasma current. With further optimization we hope to extend the β_N^* limit beyond the present value of 3.5 making the ERS mode an attractive paradigm for an advanced tokamak reactor.

In conclusion, highly peaked density and pressure profiles in a new reversed shear operating regime have been observed on TFTR. The particle transport is reduced to roughly the neoclassical level, and the ion thermal diffusivity is well below predictions from conventional neoclassical theory. The improved transport is observed throughout the region of reversed shear. Possible explanations of the inferred subneoclassical ion thermal diffusivity are the violation of the assumptions of standard neoclassical theory or a thermal pinch. Neoclassical transport is usually thought to be the minimum transport possible, and these results represent a dramatic improvement in confinement and performance. With the low transport coefficients found in the ERS mode and the predicted improvements in the stability limit, dramatic improvements in the performance of present and future tokamak reactors may be possible.

We would like to thank H. K. Park for the analysis of the density data and its uncertainties, and the TFTR staff for their support and operation of the experiment. This work was supported by United States Department of Energy Contract No. DE-AC02-76-CHO-3073.

[1] C. Kessel, J. Manickam, G. Rewoldt, and W. M. Tang, Phys. Rev. Lett. **72**, 1212 (1994).
[2] A. D. Turnbull, T. S. Taylor, Y. R. Lin-Liu, and H. S. John, Phys. Rev. Lett. **74**, 718 (1995).
[3] B. B. Kadomtsev and O. P. Pogutse, Sov. Phys. JETP **24**, 1172 (1967).
[4] M. Rosenbluth and M. L. Sloan, Phys. Fluids **14**, 1725 (1971).
[5] A. Sykes, J. A. Wesson, and S. J. Cox, Phys. Rev. Lett. **39**, 757 (1977).
[6] V. D. Shafranov, Phys. Fluids **26**, 357 (1983).
[7] R. J. Goldston *et al.*, Plasma Phys. Controlled Fusion **36**, B213 (1994).
[8] G. L. Schmidt *et al.*, in *Plasma Physics and Controlled Nuclear Fusion Research, Nice, 1988* (International Atomic Energy Agency, Vienna, 1989), Vol. I, p. 215.
[9] M. Hugon *et al.*, Nucl. Fusion **32**, 33 (1992).
[10] P. Smeulders *et al.*, Nucl. Fusion **35**, 225 (1995).
[11] D. Moreau *et al.*, in *Plasma Physics and Controlled Nuclear Fusion Research, Würzburg, 1992* (International Atomic Energy Agency, Vienna, 1993), Vol. I, p. 649.
[12] G. T. Hoang *et al.*, Nucl. Fusion **34**, 75 (1994).
[13] E. A. Lazarus *et al.*, Phys. Fluids B **3**, 2221 (1991).
[14] E. A. Lazarus *et al.*, Phys. Fluids B **4**, 3644 (1992).
[15] T. S. Taylor *et al.*, Plasma Phys. Controlled Fusion **36**, B229 (1994).
[16] S. Ishida *et al.*, Phys. Rev. Lett. **68**, 1531 (1992).
[17] J. Kesner *et al.*, Phys. Fluids B **5**, 2525 (1993).
[18] Y. Koide *et al.*, Phys. Rev. Lett. **72**, 3662 (1994).
[19] P. A. Politzer *et al.*, Phys. Plasmas **1**, 1545 (1994).
[20] J. H. Harris *et al.*, Phys. Rev. Lett. **63**, 1249 (1989).
[21] D. M. Meade and the TFTR group, in *Plasma Physics and Controlled Nuclear Fusion Research, Washington, D.C., 1990* (International Atomic Energy Agency, Vienna, 1991), Vol. I, pp. 9–24.
[22] F. M. Levinton *et al.*, Phys. Rev. Lett. **63**, 2060 (1989).
[23] F. M. Levinton, Rev. Sci. Instrum. **63**, 5157 (1992).
[24] S. P. Hirshman *et al.*, Phys. Plasmas **1**, 2277 (1994).
[25] R. J. Hawryluk, in *Proceedings of the Course in Physics of Plasmas Close to Thermonuclear Conditions, Varenna, 1979* (CEC, Brussels, 1980), Vol. I, p. 19.
[26] S. H. Batha *et al.* (to be published).
[27] J. D. Strachan *et al.*, Phys. Rev. Lett. **58**, 1004 (1987).
[28] H. K. Park, Rev. Sci. Instrum. **61**, 2879 (1990).
[29] T. K. Kurki-Suonio, R. J. Groebner, and K. H. Burrell, Nucl. Fusion **32**, 133 (1992).
[30] Z. Chang *et al.*, Phys. Rev. Lett. **74**, 4663 (1995).